

Energies and spectra of solids from the algorithmic inversion of localized GW

Tommaso Chiarotti,^{1,*} Andrea Ferretti,² and Nicola Marzari¹

¹*Theory and Simulations of Materials (THEOS) and National Centre for Computational Design and Discovery of Novel Materials (MARVEL),*

École Polytechnique Fédérale de Lausanne, 1015 Lausanne, Switzerland

²*Centro S3, CNR-Istituto Nanoscienze, 41125 Modena, Italy*

(Dated: February 24, 2023)

Energy functionals of the Green's function can provide simultaneously spectral and thermodynamic properties of interacting electrons' systems. Exploiting a localized- GW approach, we introduce an approximation to the exchange-correlation part of the Klein functional that generalizes the energy functional of DFT+ U to host a dynamical screened potential $U(\omega)$. Furthermore, we solve exactly the resulting Dyson equation extending to crystals the algorithmic-inversion method. We then compute the spectral, thermodynamic, and vibrational properties of SrVO_3 , finding results in close agreement with experiments and state-of-the-art computational methods, at very reduced computational costs.

Accurate and predictive calculations of materials properties have been and remain a challenging task [1]. Though density-functional theory (DFT) has provided a major step forward in the prediction of ground-state properties [2, 3], addressing spectroscopic quantities remains challenging [4–9]. To overcome the intrinsic limitations of DFT, dynamical methods, mostly based on Green's functions, have been used; these includes many-body perturbation theory (MPBT) approaches such as GW [10, 11], dynamical mean-field theory [12, 13] (DMFT), spectral functional theories [5, 14, 15] (SFT), and electron-boson interaction schemes [16, 17]. In all of these approaches dynamical (frequency-dependent) self-energies or potentials appear.

In Green's function theories, the Luttinger-Ward (LW) and Klein functionals [18–22] are energy functionals of the Green's function that are variational and result in conserving potentials that are dynamical. Though explicitly known diagrammatically, the exact Φ term is computationally inaccessible and needs to be approximated [23, 24]. The choice of the approximation for Φ determines the physics accessible to the functional, ranging from long-range plasmonic effects, as in GW [10, 11], to strongly-correlated local interactions as in DMFT [12, 13]. The stationarity condition of the functional yields the Dyson equation involving the interacting propagator G and the dynamical self-energy (as derivative of Φ wrt G) [21, 22]. Therefore, the functional and its derivative determine the thermodynamics and the spectral properties of a material, also allowing, at self-consistency, one to compute ground-state quantities such as forces and phonons through Hellmann-Feynman theorem [25].

Due to the presence of dynamical quantities, applications where both spectroscopic and thermodynamic quantities are computed together are limited (see Ref. [26] and references therein). In the context of GW , such calculations have been performed for model systems, such as the homogeneous electron gas [27] or Hubbard chains [28], and later extended to solids, typically us-

ing an imaginary-axis formalism [29–32]. This latter approach has been proven very effective for the prediction of ground-state properties, but retains limited accuracy for spectral properties, stemming from the analytic continuation to the real axis [33]. In the DMFT framework, an efficient implementation of a LW functional has made possible the calculation of ground-state quantities for crystals, while simultaneously accessing spectral properties [34, 35], notwithstanding the price of numerical limitations related to the cost of the solvers [13].

In the Letter, we adopt the Klein functional formalism to introduce a Φ term that generalizes the DFT+ U energy functional of Dudarev et al. [36] to host a dynamical screened potential $U(\omega)$, rather than a static U . The derivative of the functional yields the localized- GW self-energy of Ref. [37], together with a choice for the double-counting term. The resulting Dyson equation is treated as a non-linear eigenvalue problem, and solved via an exact mapping to a non-interacting system generalizing the “algorithmic inversion method on sum-over-poles” (AIM-SOP) [26] to the case of real materials. Within this approach, the single-particle Green's function, along with the Dyson orbitals and excitation energies of the system, are obtained and used to calculate accurate spectral and thermodynamic properties of the material. In addition to providing an exact solution to the Dyson equation, the procedure addresses, e.g., problems with avoided crossing in the quasi-particle solution of the Dyson equation, or numerical difficulties when integrating the Green's function to obtain thermodynamic quantities [26]. We apply this framework to the paradigmatic case study of the correlated metal SrVO_3 [38–40] finding results in very good agreement with experiments and state-of-the-art methods for the spectrum, bulk modulus, and phonons, at a greatly reduced computational cost compared to established approaches.

Algorithmic inversion method. First, we introduce a general framework to solve the Dyson equation $G(\omega) = [\omega I - h_0 - \Sigma(\omega)]^{-1}$. This task can be seen as the gen-

eralization to embedded (open) systems of the diagonalization of an Hamiltonian for closed systems. Assuming Σ to be analytical in a connected subset of the complex plane, one can exactly map the solution to the Dyson equation into the non-linear eigenvalue problem (usually shortened as NLEP [41])

$$[h_0 + \Sigma(\omega)] |\psi^r\rangle = \omega |\psi^r\rangle, \quad (1)$$

where (z_s, ψ_s^r) are the corresponding (discrete) eigenvalues and right eigenvectors. In particular, it is possible to show that the eigenvalues z_s are the poles of the resolvent $G(\omega)$, and, when poles are first-order (not granted in general), the right/left eigenvectors $|\psi_s^r\rangle \langle \psi_s^l|$ provide their residues.

Though general algorithms to solve the NLEP problem exists, we consider here the self-energy to be meromorphic (isolated poles) over the whole complex plane, and to only have first-order poles. This amounts to writing the dynamical part of the self-energy (the static contribution being included in h_0) as a sum over poles (SOP) [26, 42]:

$$\Sigma(\omega) = \sum_{m=1}^N \frac{\Gamma_m}{\omega - \Omega_m}, \quad (2)$$

resulting in a truncated Lehmann representation [42]. In Eq. (2), the amplitudes Γ_m are operators acting on the one-particle Hilbert space defined by h_0 , and $\Omega_m = \omega_m + i\delta_m$ are scalars respecting the time-ordering condition $\delta_m \geq 0$ when $\Omega_m \geq \mu$, μ being the chemical potential of the system. Within these hypotheses $G(\omega)$ can also be written exactly as a SOP, and the algorithmic inversion method (AIM) allows to obtain the coefficients of the representation, as it is for the scalar homogeneous case of Ref. [26].

Introducing a factorization of the self-energy residues $\Gamma_m = \bar{V}_m^\dagger V_m$, the Green's function reads

$$G(\omega) = \left[\omega I - h_0 - \sum_m \bar{V}_m^\dagger (\omega - \Omega_m)^{-1} V_m \right]^{-1} \quad (3)$$

which corresponds to embedding a non-interacting system h_0 and N non-interacting fictitious degrees of freedom (baths), each having an Hamiltonian $\Omega_i I_i$ and coupled to h_0 by \bar{V}_i^\dagger, V_i . Notably, the factorization of Γ_m is not unique; possible choices are $V_m = \bar{V}_m^\dagger = \Gamma_m^{1/2}$ or could be based, e.g., on the singular value decomposition (SVD) of Γ_m . By going backwards in the embedding procedure, the total Green's function of the system plus the baths is $G_{\text{tot}} = (\omega I_{\text{tot}} - H_{\text{AIM}})^{-1}$ with

$$H_{\text{AIM}} = \begin{pmatrix} h_0 & V_1 & \dots & V_N \\ \bar{V}_1^\dagger & \Omega_1 I_1 & 0 & 0 \\ \vdots & 0 & \ddots & 0 \\ \bar{V}_N^\dagger & 0 & \dots & \Omega_N I_N \end{pmatrix}; \quad (4)$$

in particular, $G(\omega) = P_0(\omega I_{\text{tot}} - H_{\text{AIM}})^{-1} P_0$, with P_0 projecting onto the h_0 Hilbert space. Importantly, the freedom in the factorization of Γ_m can be exploited to minimize the dimension of the subspaces corresponding to $I_1 \dots I_N$ (i.e. making V_m, \bar{V}_m as rectangular as possible, e.g., via a SVD), and thereby reducing the overall dimension of the H_{AIM} matrix.

At this point, while the resulting $G(\omega)$ can be expressed exactly as a SOP, it may still feature higher-order poles. This is directly connected to the question whether H_{AIM} is diagonalizable (i.e. whether it admits a complete spectral representation): in the language of nonlinear eigenvalue problems, the eigenvalues of Eq. (1) need to be semi-simple [41] for the GF to have only simple poles. In turn, this depends on the nature of the self-energy. For instance, when the poles of the self-energy Ω_m are real (with an infinitesimal offset from the real axis), and their residues Γ_m are Hermitian, the AIM matrix is Hermitian, a sufficient (but not necessary) condition for diagonalizability. In the following, the latter is assumed.

Thus, the diagonalization of H_{AIM} yields the desired SOP expression for the Green's function:

$$G(\omega) = \sum_{s=1}^{N+1} \frac{|\psi_s^r\rangle \langle \psi_s^l|}{\omega - z_s}, \quad (5)$$

where $|\psi_s^{r/l}\rangle$ are the right/left eigenvectors of Eq. (1) computed, according to the above discussion, as the projections of the linear H_{AIM} eigenvectors on the P_0 manifold, and with z_s their eigenvalues. We have thus turned a non-linear eigenvalue problem into a linear one in a larger space. Hence, starting from the poles and residues of the self-energy this algorithmic inversion provides excitation energies, lifetimes, and amplitudes (Dyson orbitals) of the system, i.e., the real and imaginary part of the poles and their residues. Furthermore, the knowledge of the Green's function as SOP allows for the analytic calculations of its moments and thus for the evaluation of integrated thermodynamic quantities [26]. This approach is the generalization to the non-homogeneous case of Ref. [26], in which the homogeneous electron gas was considered. Mathematically, AIM can be viewed as a special case of the ‘‘linearization’’ treatment of NLEP using rational functions [41]. In Ref. [43] a similar construction was used to efficiently invert the Dyson equation in the context of DMFT, with applications in Refs. [13, 44, 45]. Related approaches have also appeared recently to efficiently compute the GW self-energy and solve the Bethe-Salpeter equation [46, 47].

Localized-GW functional. Taking AIM-SOP as a formal and effective way to solve electronic-structure problems subject to dynamical potentials, here we introduce a functional formulation that generalizes the DFT+U energy functional of Dudarev et al. [36] to host a frequency-

dependent screened potential $U(\omega)$. In particular, we write a localized- GW Klein energy functional

$$E_{GW_{\text{Loc}}}[G] = E_H[\rho] + E_{xc}[\rho] + \Phi_{GW_{\text{Loc}}}[\mathbf{G}] \quad (6)$$

$$- \text{Tr}_\omega [G_0^{-1}G] + \text{Tr}_\omega \text{Log } G_0^{-1}G + \text{Tr}_\omega [h_0 G_0],$$

where $\text{Tr}_\omega[\dots]$ stands for $\int \frac{d\omega}{2\pi i} e^{i\omega 0^+} \text{Tr}[\dots]$, $G_0^{-1} = \omega I - h_0$, G is the Green's function of the system, ρ is the density of G , and \mathbf{G} is the projection of G onto a localized manifold of electronic states (noted as Hubbard manifold). For a single site the generalized Hubbard energy functional reads:

$$\Phi_{GW_{\text{Loc}}}[\mathbf{G}] = \frac{1}{2} \int \frac{d\omega}{2\pi i} \frac{d\omega'}{2\pi i} e^{i\omega 0^+} e^{i\omega' 0^+} U(\omega') \times \quad (7)$$

$$\times \text{Tr} \left\{ \mathbf{G}(\omega + \omega') [\delta(\omega - c)\mathbf{I} - \mathbf{G}(\omega)] \right\}$$

with $U(\omega)$ being the screened potential $W(\omega)$ of the system projected onto the localized space and averaged over it, and c a constant aimed to address double counting.

$\Phi_{GW_{\text{Loc}}}[\mathbf{G}]$ then yields the time-ordered self-energy

$$\Sigma_{GW_{\text{Loc}}}(\omega) = 2\pi i \frac{\delta \Phi_{GW_{\text{Loc}}}[\mathbf{G}]}{\delta \mathbf{G}} \quad (8)$$

$$= - \int \frac{d\omega'}{2\pi i} e^{i\omega' 0^+} U(\omega') \mathbf{G}(\omega + \omega') + \frac{1}{2} U(c) \mathbf{I},$$

which is composed by the localized- GW self-energy [37] (first term), and a double-counting term $\frac{1}{2}U(c)\mathbf{I}$. Here, we fix the double counting parameter c as $c \rightarrow \infty$, so that $U(c) = U_\infty$, in agreement with Ref. [48]. Importantly, we note that $\Phi_{GW_{\text{Loc}}}$ reduces to the DFT+U Hubbard energy term of Ref. [36] when a static screened local interaction U is considered. In addition, $\Phi_{GW_{\text{Loc}}}$ reduces to the GW_0 functional (plus a double-counting term) in the limit of the Hubbard manifold becoming the entire crystal. The generalization to multiple sites consists in summing different Φ^I terms, one per site, and is not treated here for simplicity.

Being a Klein functional with the screened interaction set to $U(\omega)$, $E_{GW_{\text{Loc}}}[G]$ can be made stationary by solving self-consistently the corresponding Dyson equation with a static term $h_0 = h_{\text{KS}}(\rho)$ and a self-energy

$$\Sigma_{GW_{\text{Loc}}}(\omega) = \sum_{m,m'} |\phi_m\rangle \Sigma_{GW_{\text{Loc}}}^{mm'}(\omega) \langle \phi_{m'}|,$$

where $\{\phi_m\}$ span the localized Hubbard space. Here, the use of the algorithmic inversion method is crucial and provides a ‘‘closed’’ formulation with respect to the SOP form for the propagators. Starting with an initial Green's function expressed on SOP, e.g., $G = G_{\text{KS}}$, and a SOP for the screened interaction $U(\omega)$, the self-energy $\Sigma_{GW_{\text{Loc}}}$ of Eq. (8), and consequently also $\Sigma_{GW_{\text{Loc}}}$, can be written as a SOP, since the convolution of two SOPs is a SOP [26] and the projections are just linear operations on

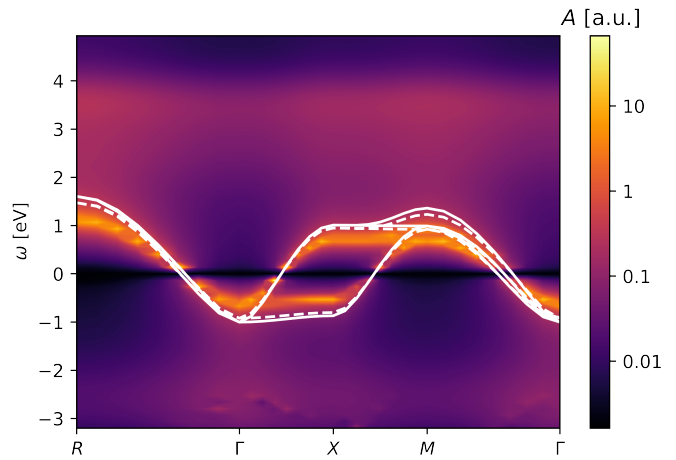


FIG. 1. Spectral function of SrVO_3 from this work (color plot) compared to PBEsol (solid white line) and PBEsol+U (dashed white line). Only the t_{2g} bands are displayed. The chemical potential is shifted to 0 in all three cases. The thin black band at 0 stems from the analytic divergence of the spectral function in a metal at the chemical potential. The color map is logarithmic.

the residues. With a self-energy on SOP, the algorithmic-inversion method can be used to find the SOP for the Green's function. The cycle can then be iterated until self-consistency. Furthermore, the SOP form of the Green's function naturally allows for the accurate evaluation of the generalized Hubbard energy of Eq. (7), the chemical potential, and in general integrated thermodynamic quantities [26].

Application to SrVO₃. As a case study, we apply the formalism to the paradigmatic example of SrVO_3 , where localized- GW has already been proven to give qualitative good spectral results [37]. Here, we provide not only the spectral properties of the material but also integrated quantities, such as the total energy and its derivatives (lattice parameter, bulk modulus, phonons), obtained from the functional $E_{GW_{\text{Loc}}}[G]$. Note that in the Letter we choose a correlated metal, though the framework can be readily applied also to correlated gapped materials. As mentioned, a choice of $U(\omega)$, accounting for the dynamical screening of the electrons in the Hubbard localized manifold, is needed, and given the localized- GW nature of the self-energy, and thus of the functional, we have considered $U(\omega)$ to be the average over the Hubbard space of the screened interaction W in the random-phase approximation; further details are given in the Supplemental Material [49].

Though designed for self-consistency, here we limit the approach to a one-shot calculation — i.e., a single-step in the stationarization of $E_{GW_{\text{Loc}}}$ — using as starting propagator the self-consistent Kohn-Sham Green's function computed with standard semi-local (PBEsol) DFT [50]. By doing so, we need to evaluate the energy functional

Method	BW	m^*/m_{PBEsol}	LS	US
PBEsol	1.0	1		
PBEsol + U	0.92	1.1		
GW+DMFT [38]	0.5	2	-1.6	2
GW+DMFT [51]	0.6	2	-1.5	2.5
GW+EDMFT [40]			-1.7	2.8
This work	0.6	2	-1.7	2.2
exp. [52]	0.7	1.8	-1.5	
exp. [53]	0.44	2	-1.5	

TABLE I. Occupied bandwidth (BW) of the t_{2g} bands, the mass enhancement factor (m^*/m_{PBEsol}), and energy of the lower (LS) and upper satellites (US) from experiments and different theoretical frameworks. Results from the generalized dynamical Hubbard functional introduced in this work are estimated from the spectral function in Fig 1. m^*/m_{PBEsol} is estimated using the ratio of the full bandwidths (LDA and PBEsol coincide). All energies are in eV.

at $E_{G_{W_{\text{Loc}}}}[G = G_{\text{KS}}]$, and the same for the self-energy, $\Sigma_{G_{W_{\text{Loc}}}}[G = G_{\text{KS}}]$. Exploiting the algorithmic-inversion method we find the non-self-consistent Green's function. At this level, the localized-GW Klein energy functional simplifies to $E_{G_{W_{\text{Loc}}}}[G_{\text{KS}}] = E_{\text{DFT}}[\rho] + \Phi_{G_{W_{\text{Loc}}}}[\mathbf{G}_{\text{KS}}]$, correcting the DFT energy with a generalized dynamical Hubbard energy term. The numerical details of the calculations are given in the Supplemental Material [49].

In Fig. 1 we show the spectral function resulting from the calculations. Contrary to DFT (PBEsol), or DFT+U (PBEsol+U), that only shifts the chemical potential, the spectral function originating from $\Sigma_{G_{W_{\text{Loc}}}}$ shows a reduction of the bandwidth along with a renormalization of the full width of the t_{2g} bands. In Tab. I we report the bandwidth (BW), the mass enhancement factor (m^*/m_{PBEsol}), and the positions of the lower/upper satellites (LS/US). While PBEsol and PBEsol+U overestimate occupied and full bandwidth, the present results reproduce the data of Ref. [37] from localized-GW and are in very good agreement with experiments [52, 53] and DMFT [38, 40, 51].

From the knowledge of the SOP of the Green's function (here KS) and the functional form of $\Phi_{G_{W_{\text{Loc}}}}$, we can straightforwardly calculate total energies and total-energy differences. In Fig. 2 we compare the equation of state for SrVO₃ as obtained from PBEsol, PBEsol+U, and the present dynamical formulation. In the legend we report the estimated values for the equilibrium volume V and the bulk modulus B , using a Birch-Murnagan third-order function for the fitting [55]. It can be observed that the present approach correctly predicts the softening of the bulk modulus, while over correcting the equilibrium lattice parameter, which can be attributed to the lack of self consistency in the calculations. In the Supplemental Material [49] we analyze the softening of the bulk modulus

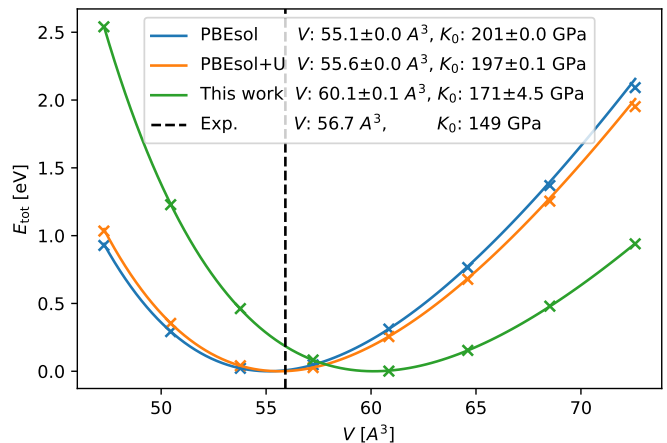


FIG. 2. Equation of state for SrVO₃ calculated using PBEsol (blue), PBEsol+U (orange), and the present approach (green). Data (crosses) are fitted using the Birch-Murnaghan curve (in solid). The values and errors obtained using the fit are displayed in the legend. For reference, in dashed black we mark the experimental volume, and report the bulk modulus in the legend. Experimental values are taken from [54].

(THz)	PBEsol	LDA+EDMFT [35]	This work
ω_1	4.86	4.3	3.9
ω_2	10.3	9.0	9.4
ω_3	11.0	11.2	12.1
ω_4	17.3	18.9	19.4

TABLE II. Zone center phonons for SrVO₃ calculated with different approaches; the last column shows the results obtained using the generalized dynamical functional introduced in this work (on top of PBEsol). The data from Ref. [35] have been estimated from the plot.

in terms of charge rearrangement.

Finally, using the relaxed structures, and taking advantage of the inexpensive computational cost of the present method, we report in Tab. II the zone-center phonons for SrVO₃. Since the Hellmann-Feynman theorem does not apply due to the lack of self-consistency, we evaluate the forces for the different displacements of the atoms with finite total energy differences. In line with the softening of the bulk modulus, the first two frequencies are lowered wrt PBEsol calculations. Also, similarly to state-of-the-art methods such as LDA+EDMFT [35] the remaining optical modes are shifted higher in frequency.

In conclusion, in the Letter we provide a computationally straightforward Green's function framework to address the electronic structure in correlated materials using dynamical potentials. First, we link the solution of Dyson-like equations to non-linear eigenvalue problems, and solve them extending the algorithmic inversion method on sum over poles (AIM-SOP) of Ref. [26] to realistic materials. Then, we present an approximation to the exchange-correlation Φ part of the energy Klein func-

tional, yielding a localized- GW self-energy, and providing a dynamical generalization of DFT+U. Though not aiming to treat strong correlations, we combine this functional with the algorithmic-inversion method to study the paradigmatic case of SrVO_3 , showing results that are close to state-of-the-art computational approaches, but with a modest computational cost, and accessing simultaneously spectral and thermodynamic properties (total energies and differences). Moreover, the existence of a Klein functional guarantees the possibility to perform self-consistent calculations, and thus to use the Hellmann-Feynman theorem to calculate forces in a Green's function formalism. Further refinements of the dynamical functional can also be investigated.

We acknowledge stimulating discussions with Mario Caserta and Marco Vanzini. This work was supported by the Swiss National Science Foundation (SNSF) through grant No. 200021-179138 (T.C.) and NCCR MARVEL (N.M.), a National Centre of Competence in Research through grant No. 205602, and from the EU Commission for the MaX Centre of Excellence on 'Materials Design at the eXascale' under grant No. 101093374 (A.F., N.M.).

* corresponding author: tommaso.chiarotti@epfl.ch

- [1] N. Marzari, A. Ferretti, and C. Wolverton, *Nature Materials* **20**, 736 (2021).
- [2] P. Hohenberg and W. Kohn, *Physical Review* **136**, B864 (1964).
- [3] W. Kohn and L. J. Sham, *Physical Review* **140**, A1133 (1965).
- [4] G. Borghi, A. Ferretti, N. L. Nguyen, I. Dabo, and N. Marzari, *Physical Review B* **90**, 075135 (2014).
- [5] A. Ferretti, I. Dabo, M. Cococcioni, and N. Marzari, *Physical Review B* **89**, 195134 (2014).
- [6] J. P. Perdew, W. Yang, K. Burke, Z. Yang, E. K. U. Gross, M. Scheffler, G. E. Scuseria, T. M. Henderson, I. Y. Zhang, A. Ruzsinszky, H. Peng, J. Sun, E. Trushin, and A. Görling, *Proceedings of the National Academy of Sciences* **114**, 2801 (2017).
- [7] N. L. Nguyen, N. Colonna, A. Ferretti, and N. Marzari, *Physical Review X* **8**, 021051 (2018).
- [8] R. De Gennaro, N. Colonna, E. Linscott, and N. Marzari, *Physical Review B* **106**, 035106 (2022).
- [9] N. Colonna, R. De Gennaro, E. Linscott, and N. Marzari, *Journal of Chemical Theory and Computation* **18**, 5435 (2022).
- [10] L. Hedin and S. Lundqvist, in *Solid State Physics*, Vol. 23, edited by F. Seitz, D. Turnbull, and H. Ehrenreich (Academic Press, 1970) pp. 1–181.
- [11] L. Reining, *Wiley Interdisciplinary Reviews: Computational Molecular Science* **8**, e1344 (2018).
- [12] A. Georges, G. Kotliar, W. Krauth, and M. J. Rozenberg, *Reviews of Modern Physics* **68**, 13 (1996).
- [13] G. Kotliar, S. Y. Savrasov, K. Haule, V. S. Oudovenko, O. Parcollet, and C. A. Marianetti, *Reviews of Modern Physics* **78**, 865 (2006).
- [14] S. Y. Savrasov and G. Kotliar, *Physical Review B* **69**, 245101 (2004).
- [15] M. Vanzini, A. Aouina, M. Panholzer, M. Gatti, and L. Reining, *npj Computational Materials* **8**, 1 (2022).
- [16] F. Caruso, C. Verdi, S. Poncé, and F. Giustino, *Physical Review B* **97**, 165113 (2018).
- [17] J. S. Zhou, L. Reining, A. Nicolaou, A. Bendounan, K. Ruotsalainen, M. Vanzini, J. J. Kas, J. J. Rehr, M. Muntwiler, V. N. Strocov, F. Sirotti, and M. Gatti, *Proceedings of the National Academy of Sciences* **117**, 28596 (2020).
- [18] J. M. Luttinger and J. C. Ward, *Physical Review* **118**, 1417 (1960).
- [19] G. Baym and L. P. Kadanoff, *Physical Review* **124**, 287 (1961).
- [20] G. Baym, *Physical Review* **127**, 1391 (1962).
- [21] R. M. Martin, L. Reining, and D. M. Ceperley, *Interacting Electrons: Theory and Computational Approaches* (2016).
- [22] G. Stefanucci and R. v. Leeuwen, *Nonequilibrium Many-Body Theory of Quantum Systems: A Modern Introduction* (2013).
- [23] C.-O. Almbladh, U. V. Barth, and R. V. Leeuwen, *International Journal of Modern Physics B* **13**, 535 (1999).
- [24] N. E. Dahlen and U. v. Barth, *Physical Review B* **69**, 195102 (2004).
- [25] K. Haule and G. L. Pascut, *Physical Review B* **94**, 195146 (2016).
- [26] T. Chiarotti, N. Marzari, and A. Ferretti, *Physical Review Research* **4**, 013242 (2022).
- [27] B. Holm and U. von Barth, *Physical Review B* **57**, 2108 (1998).
- [28] A. Honet, L. Henrard, and V. Meunier, *AIP Advances* **12**, 035238 (2022).
- [29] A. Kutepov, S. Y. Savrasov, and G. Kotliar, *Physical Review B* **80**, 041103 (2009).
- [30] A. Kutepov, K. Haule, S. Y. Savrasov, and G. Kotliar, *Physical Review B* **85**, 155129 (2012).
- [31] M. Grumet, P. Liu, M. Kaltak, J. c. v. Klimeš, and G. Kresse, *Phys. Rev. B* **98**, 155143 (2018).
- [32] C.-N. Yeh, S. Isakov, D. Zgid, and E. Gull, *Physical Review B* **106**, 235104 (2022).
- [33] A. L. Kutepov and G. Kotliar, *Physical Review B* **96**, 035108 (2017).
- [34] K. Haule and T. Birol, *Physical Review Letters* **115**, 256402 (2015).
- [35] C. P. Kocçer, K. Haule, G. L. Pascut, and B. Monserrat, *Physical Review B* **102**, 245104 (2020).
- [36] S. L. Dudarev, G. A. Botton, S. Y. Savrasov, C. J. Humphreys, and A. P. Sutton, *Physical Review B* **57**, 1505 (1998).
- [37] T. Miyake, C. Martins, R. Sakuma, and F. Aryasetiawan, *Physical Review B* **87**, 115110 (2013).
- [38] J. M. Tomczak, M. Casula, T. Miyake, and S. Biermann, *Physical Review B* **90**, 165138 (2014).
- [39] R. Sakuma, C. Martins, T. Miyake, and F. Aryasetiawan, *Physical Review B* **89**, 235119 (2014).
- [40] L. Boehnke, F. Nilsson, F. Aryasetiawan, and P. Werner, *Physical Review B* **94**, 201106 (2016).
- [41] S. Güttel and F. Tisseur, *Acta Numerica* **26**, 1 (2017).
- [42] G. E. Engel, B. Farid, C. M. M. Nex, and N. H. March, *Physical Review B* **44**, 13356 (1991).
- [43] S. Y. Savrasov, K. Haule, and G. Kotliar, *Physical Review Letters* **96**, 036404 (2006).
- [44] L. Wang, H. Jiang, X. Dai, and X. C. Xie, *Physical Re-*

- view B **85**, 235135 (2012).
- [45] J. C. Budich, R. Thomale, G. Li, M. Laubach, and S.-C. Zhang, *Physical Review B* **86**, 201407 (2012).
- [46] S. J. Bintrim and T. C. Berkelbach, *The Journal of Chemical Physics* **154**, 041101 (2021).
- [47] Y. Cho, S. J. Bintrim, and T. C. Berkelbach, *Journal of Chemical Theory and Computation* **18**, 3438 (2022).
- [48] M. Vanzini and N. Marzari, in preparation (2023).
- [49] See Supplemental Material for computational details and further discussion of the theoretical approach adopted.
- [50] J. P. Perdew, K. Burke, and M. Ernzerhof, *Physical Review Letters* **77**, 3865 (1996).
- [51] R. Sakuma, P. Werner, and F. Aryasetiawan, *Physical Review B* **88**, 235110 (2013).
- [52] T. Yoshida, K. Tanaka, H. Yagi, A. Ino, H. Eisaki, A. Fujimori, and Z.-X. Shen, *Physical Review Letters* **95**, 146404 (2005).
- [53] M. Takizawa, M. Minohara, H. Kumigashira, D. Toyota, M. Oshima, H. Wadati, T. Yoshida, A. Fujimori, M. Lippmaa, M. Kawasaki, H. Koinuma, G. Sordi, and M. Rozenberg, *Physical Review B* **80**, 235104 (2009).
- [54] T. Maekawa, K. Kurosaki, and S. Yamanaka, *Journal of Alloys and Compounds* **426**, 46 (2006).
- [55] F. Birch, *Physical Review* **71**, 809 (1947).

Supplemental Material: Energies and spectra of solids from the algorithmic inversion of localized GW

Tommaso Chiarotti,^{1,*} Andrea Ferretti,² and Nicola Marzari¹

¹*Theory and Simulations of Materials (THEOS) and National Centre for Computational Design and Discovery of Novel Materials (MARVEL), École Polytechnique Fédérale de Lausanne, 1015 Lausanne, Switzerland*

²*Centro S3, CNR-Istituto Nanoscienze, 41125 Modena, Italy*

(Dated: February 24, 2023)

This document contains the supplemental material for the paper: “Energies and spectra of solids from the algorithmic inversion of localized GW ”.

CONTENTS

S1. From static U to dynamical $U(\omega)$	1
S2. From GW to localized- GW	2
S3. Numerical details	2
S4. Charge rearrangement within localized GW	3
References	4

S1. FROM STATIC U TO DYNAMICAL $U(\omega)$

Similarly to choosing the screening parameter U in DFT+U, a choice of $U(\omega)$, accounting for the dynam-

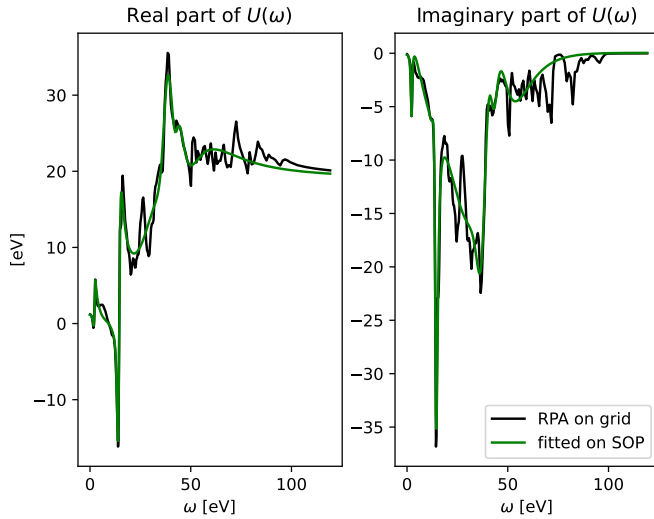


FIG. S1. Real and imaginary part of the localized screened interaction $U(\omega)$ calculated on a frequency grid using the random-phase approximation (black line) compared to its representation in a sum-over-poles form (green line) obtained using a non-linear least squared minimization technique.

ical screening of the electrons in the Hubbard localized manifold, is required. In the spirit of localized GW and Ref. [1], we calculate the screening for the Hubbard site I as the manifold average

$$U(\omega) = \frac{1}{N_I^2} \sum_{m,m'} W_{Im,Im'}^{Im',Im}, \quad (\text{S.1})$$

$$W_{Im,Im'}^{Im',Im} = \int d\mathbf{r}d\mathbf{r}' \phi_{Im'}^*(\mathbf{r})\phi_{Im}^*(\mathbf{r}') W(\mathbf{r},\mathbf{r}') \times \phi_{Im}(\mathbf{r})\phi_{Im'}(\mathbf{r}'), \quad (\text{S.2})$$

with W calculated within the random-phase approximation, and m being the orbital index of localized functions centred on the site I , e.g., atomic projectors or maximally localized Wannier functions [2]. For SrVO_3 we choose the vanadium as the active Hubbard site, and ortho-atomic projectors as localized functions.

After being calculated on grid, $U(\omega)$ is transformed to a SOP using a mixed linear and non-linear least square minimization on the cost function

$$C = \sum_j \left| U(\omega_j) - \sum_l \frac{A_l}{\omega_j - g_l} \right|^2, \quad (\text{S.3})$$

where at each step of the minimization the real coefficients A_l are found with a generalized linear least-square approach [3], and the complex (time-ordered) poles g_l with a simulated annealing on C using the newly found amplitudes. Such an algorithm requires an initial guess of the real (position) and imaginary (broadening) parts of the poles, and, at each step, is required to not move them by at most 10% of their value. The algorithm has been shown to be robust with respect to changes of the initial values.

In Fig. S1 we show the real (left) and imaginary (right) parts of the calculated RPA screened interaction (black lines) compared to the result of the fitting procedure (green lines), having chosen 10 poles for the fit. The agreement is excellent at lower energies ($\omega < 25$ eV) and slightly worsen afterwards. Still, the error in the two limits $\omega \rightarrow 0$ and $\omega \rightarrow \infty$ (300 eV) is of the order of 10 meV, and thus quite low.

* corresponding author: tommaso.chiarotti@epfl.ch

S2. FROM GW TO LOCALIZED-GW

In this section we show that

$$\Sigma_{GW_{\text{Loc}}} = - \int \frac{d\omega'}{2\pi i} e^{i\omega'0^+} U(\omega') \mathbf{G}(\omega + \omega') \quad (\text{S.4})$$

can be seen as a localized form of the *GW* self-energy,

$$\Sigma(\mathbf{r}, \mathbf{r}', \omega) = - \int \frac{d\omega'}{2\pi i} e^{i\omega'0^+} G(\mathbf{r}, \mathbf{r}', \omega + \omega') W(\mathbf{r}, \mathbf{r}', \omega). \quad (\text{S.5})$$

This approach has been adapted from Ref. [1] and is similar to Refs. [4, 5].

In the following we make use of the Lehmann representation of the Green's function,

$$G(\mathbf{r}, \mathbf{r}', \omega) = \sum_s \frac{\psi_s(\mathbf{r}) \psi_s^*(\mathbf{r}')}{\omega - \epsilon_s \pm i0^+}, \quad (\text{S.6})$$

where $\psi_s(\mathbf{r})$ are the Dyson orbitals, ϵ_s the charged excitations of the material, and $\pm i0^+$ provide the correct time ordering of the propagator. On a localized basis around a site I (labelled here with Greek letters like α, β, γ) the self energy reads

$$\langle \alpha | \Sigma(\omega) | \beta \rangle = - \sum_s \int \frac{d\omega'}{2\pi i} e^{i\omega'0^+} \int d\mathbf{r} d\mathbf{r}' \left[\frac{\psi_s(\mathbf{r}) \alpha^*(\mathbf{r}) W(\mathbf{r}, \mathbf{r}', \omega) \beta(\mathbf{r}') \psi_s^*(\mathbf{r}')}{\omega + \omega' - \epsilon_s \pm i0^+} \right]. \quad (\text{S.7})$$

Introducing the four-point notation for the screened potential [6]

$$W_{\alpha\beta}^{ss}(\omega) = \int d\mathbf{r} d\mathbf{r}' \alpha^*(\mathbf{r}) \psi_s(\mathbf{r}) W(\mathbf{r}, \mathbf{r}', \omega) \beta(\mathbf{r}') \psi_s^*(\mathbf{r}'), \quad (\text{S.8})$$

the self-energy can be rewritten as

$$\langle \alpha | \Sigma(\omega) | \beta \rangle = - \sum_s \int \frac{d\omega'}{2\pi i} e^{i\omega'0^+} \frac{W_{\alpha\beta}^{ss}(\omega)}{\omega + \omega' - \epsilon_s \pm i0^+}. \quad (\text{S.9})$$

Then, as in Refs. [1, 4, 5], we separate each Dyson orbital into an itinerant (delocalized) component and a localized one, $|\psi_s\rangle = |s_{\text{it}}\rangle + \sum_\gamma |\gamma\rangle \langle \gamma | s \rangle$. The screened potential is separated in

$$W_{\alpha\beta}^{ss}(\omega) = W_{\alpha\beta}^{s_{\text{it}}s_{\text{it}}}(\omega) + \sum_\gamma \left[W_{\alpha\beta}^{\gamma s_{\text{it}}}(\omega) + W_{\alpha\beta}^{s_{\text{it}}\gamma}(\omega) \right] + \sum_{\gamma, \gamma'} W_{\alpha\beta}^{\gamma\gamma'}(\omega), \quad (\text{S.10})$$

where, since we suppose the screened interaction to be short-range, we discard the first three terms. Owing to the localization of the basis of the site, we can approxi-

mate the fourth term as [5]:

$$W_{\alpha\beta}^{\gamma\gamma'}(\omega) = \int d\mathbf{r} d\mathbf{r}' \alpha^*(\mathbf{r}) \gamma^*(\mathbf{r}') W(\mathbf{r}, \mathbf{r}') \gamma(\mathbf{r}) \beta(\mathbf{r}') \approx \delta_{\alpha\gamma'} \delta_{\gamma\beta} W_{\alpha\beta}^{\beta\alpha}(\omega). \quad (\text{S.11})$$

Discarding the three terms in Eq. (S.10), and using Eq. (S.11), we can write the localized form of the self-energy from Eq. (S.9)

$$\langle \alpha | \Sigma_{GW_{\text{Loc}}}(\omega) | \beta \rangle = - \int \frac{d\omega'}{2\pi i} e^{i\omega'0^+} \sum_s \frac{\langle \alpha | s \rangle \langle s | \beta \rangle}{\omega + \omega' - \epsilon_s \pm i0^+} W_{\alpha\beta}^{\beta\alpha}(\omega). \quad (\text{S.12})$$

Calling $|\alpha\rangle = |I, m\rangle$ and $|\beta\rangle = |J, m'\rangle$, together with discarding off site contributions—those terms would give a $+V$ -like term [1]—, and averaging the on site terms m, m' , as in Eq. (S.1), the localized-GW self-energy reads as in Eq. (S.4), for a single site.

S3. NUMERICAL DETAILS

All DFT and DFT+U calculations are performed using the PWscf code of QUANTUM ESPRESSO distribution [7]. The energy, self-energy, Green's function, and spectral function, are computed with a PYTHON implementation of the generalized Hubbard approach described in the main text. The localized screened-potential $U(\omega)$ has been calculated using RESPACK [8] using maximally localized projectors. The pseudopotentials used for all the calculations are optimized norm-conserving pseudopotentials [9] (PBEsol standard-precision, nc-sr-04) from the PSEUDO DOJO library [10]. The phonon calculations have been performed with the help of PHONOPY [11, 12] to compute the energy differences. The sum-over-poles form for $U(\omega)$ is found using an in-house PYTHON implementation of the algorithm described in Sec. S1.

For the calculations in Figs. 1 (main text) and S2 (Supp. Mater.), and Table I (main text), i.e., all but those for the equation of state (EOS), we use a simple cubic cell having a lattice parameter of $a = 3.824$ Å. This is the extrapolated value at the zero-temperature limit of the experimental value $a = 3.841$ Å from Refs. [13] and [14], considering an average linear thermal expansion coefficient $\alpha_l = 1.45 \times 10^{-5} K^{-1}$ from Ref. [13].

For all electronic structure calculations we use a Marzari-Vanderbilt [15] smearing of ~ 0.27 eV. For the generalized Hubbard calculations, involving G_{KS} , we shift the poles above and below the real axis with an effective amount of $i\eta_\pm = \pm i 0.1$ eV, according to whether the pole is occupied (+) or empty (−). To implement the smearing in G_{KS} , we double each pole to be both above and below the real axis multiplying its occupation—1 in the Kohn and Sham basis—, by a factor $f^\pm(1-f^\pm)$ where + is the sign of η_\pm . Here, f^\pm is the Marzari-Vanderbilt

smearing function, and $f^- = 1 - f^+$.

For all total energy and ground-state density calculations—DFT, DFT+U, and generalized Hubbard—, we use a $12 \times 12 \times 12$ \mathbf{k} -points Monkhorst-Pack grid. Specifically, this \mathbf{k} -grid is used to compute E_{tot} in the lines “DFT, DFT+U, This work” of Table I, as well as the equation of state of Fig. 2 and the charge-density differences of Fig. S2. With the chosen values we assure a 10 meV (or better) convergence on the total-energy in DFT.

Due to the \mathbf{k} -point sampling, the localized-GW approach needs an additional “pole-condensation” procedure. The issue originates from the number of poles of the self-energy, which scales linearly with the dimension of the H_{AIM} that we need to diagonalize. The self-energy poles are calculated from Eq. (8), i.e. using the SOP form for \mathbf{G} and U . Specifically, the number of poles of Σ is equal to the number of poles of \mathbf{G} times those of U . While U brings in a number of poles in the order of 10, the projected KS Green’s function has poles at all KS states with residues as projections over the Hubbard manifold,

$$\mathbf{G}_{mm'}^{\text{KS}}(\omega) = \sum_{\mathbf{k}, n} \frac{\langle m | \psi_{n\mathbf{k}} \rangle \langle \psi_{n\mathbf{k}} | m' \rangle}{\omega - \epsilon_{n\mathbf{k}} + i\eta_{\pm}}, \quad (\text{S.13})$$

where $|m\rangle$ span the Hubbard manifold, and $\psi_{n\mathbf{k}}, \epsilon_{n\mathbf{k}}$ are the Kohn-Sham orbitals and eigenvalues. The sum is performed on all the Kohn-Sham states. Thus, with a $12 \times 12 \times 12$ grid and 25 orbitals in the calculation, one gets more than 10000 poles (without enforcing point-group symmetries). As it happens for the density of states, when projected to the localized manifold most of these poles effectively overlap, giving a structure that can be then represented with much fewer poles.

In order to condense the poles we adopt a strategy inspired from the weighted-mean of N random variables. Indeed, one can see the spectral function of a sum-over-poles representation of a propagator, i.e., the absolute value of the imaginary part, as a distribution function. In SOP, this must be a sum of Lorentzians [16] each centred at $\epsilon_{n\mathbf{k}}$ and broadened by η . Then, if the overlap of two Lorentzians is greater than a threshold the two poles can be regarded effectively as one. In particular:

- We sequentially browse the (ordered) pole array.
- We compare the weighted-mean of the first two (real part of the) poles — having a weight equal to each broadening — and compare it with the first.
- If the separation between the position (real part) of the two poles is less than a threshold, we replace them with a newly defined pole, with a position equal to the weighted mean, broadening as the weighted mean variance, and residue (or amplitude [16]) as the sum of the two.
- We continue with the rest of the poles.

We do this procedure separately for the four quarters of the complex plane, defined by the real axis and the position of the chemical potential. Please note that this procedure preserves the normalization of the Green’s function — since we are summing the amplitudes —, and preserves the total number of particles, since we are doing it for occupied and empty poles separately. We check that the value chosen for the threshold changes the total energy for less than 10 meV. With this procedure, we are able to reduce the number of poles to a few hundreds (without symmetries), making the diagonalization of H_{AIM} computationally much cheaper.

In addition to the total energy, within these settings we also calculate the density matrix, then used e.g. in Fig. S2, using a chemical potential that solves:

$$N = \int_{-\infty}^{\mu} d\omega \text{Tr} A(\omega), \quad (\text{S.14})$$

where $A(\omega)$ is the spectral function and the integral is done analytically thanks to the SOP form of G . For the spectral properties — Fig. 1, and the values in the lines “DFT, DFT+U, This work” of Table I — we use a denser Monkhorst-Pack grid of $16 \times 16 \times 16$ \mathbf{k} -points. For DFT and DFT+U we use the self-consistent density calculated with the coarser grid. For generalized Hubbard, according to [16], we solve the Dyson equation,

$$G^{-1}(\omega) = G_0^{-1}(\omega) - \Sigma(\omega) + \mu, \quad (\text{S.15})$$

with μ calculated from Eq. (S.14), on the \mathbf{k} -path of Fig. 1, using again the algorithmic inversion. The bandwidth in Table I is calculated at the Γ point, considering the peak (in frequency) of the spectral function, for the dynamical Hubbard approach. The numerical value of the mass enhancement factor is computed by dividing the full bandwidth of the method, by the DFT value.

S4. CHARGE REARRANGEMENT WITHIN LOCALIZED GW

To get a qualitative picture concerning the lowering of the bulk-modulus of SrVO_3 when applying the localized GW approach, in Fig. S2 we compare charge-density differences from different methods along the (100) plane. On the plane, vanadium atoms are on the corners, and oxygens on the midpoint of the cell. The color-code in the plots is red-green-blue, with red being positive, green zero, blue negative. In panel S2a, one can see the comparison between the DFT and DFT+U charge densities. Looking at the left corner, one can see that there is no qualitative change in the charge density at the middle of the bond between the vanadium and the oxygen atoms. Conversely, in the other two plots, the DFT (panel S2b) or the DFT+U (panel S2c) charge in the middle is pulled toward the atoms. Effectively, this can account for a lowering of the bulk-modulus as obtained by the localized-GW approach with respect to DFT and

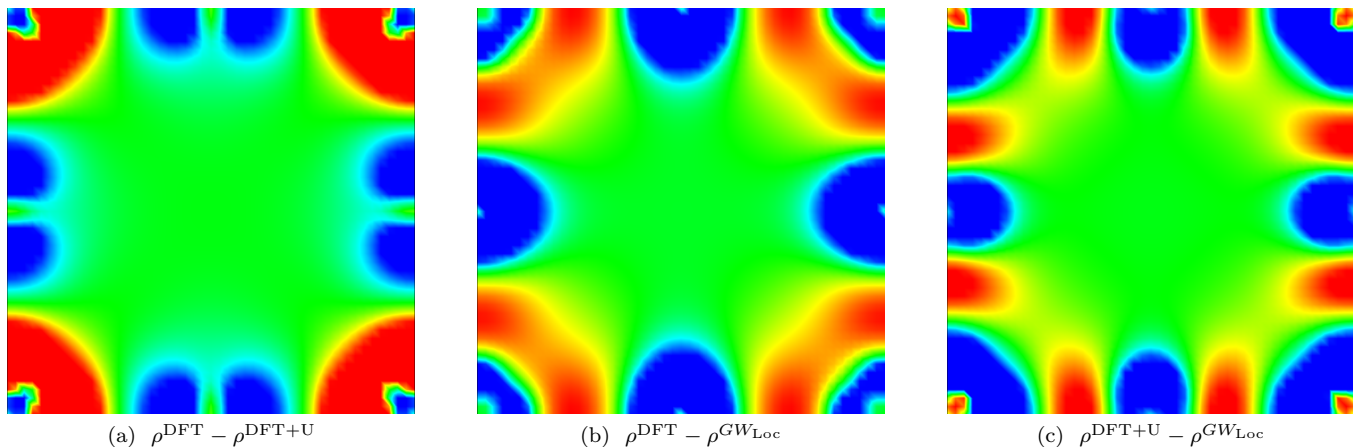


FIG. S2. Comparison between charge-density differences from different methods along the 100 plane on SrVO₃. In the cell, vanadium atoms are on the corners, oxygen atoms are on the midpoint of each edge, and strontium is at the center of the cell and cannot be seen from the plot since in the center of the cell and we are cutting with a plane on the surface of the cell. All calculations are done at the experimental equilibrium ($T = 0$ limit) lattice parameter of SrVO₃, see the text for more details. The color-coding is red-green-blue, with red being positive, green zero, blue negative. Same color for different plots are the same value. For example, in panel (b) the zone where is red ρ^{DFT} is higher than ρ^{GWLoc} , where is blue is viceversa, and where is green the system has the same electronic charge density.

DFT+U. Also, since the Hubbard manifold is around the

vanadium atom, no changes in the charge density on the strontium are observed.

-
- [1] M. Vanzini and N. Marzari, in preparation (2023).
- [2] N. Marzari, A. A. Mostofi, J. R. Yates, I. Souza, and D. Vanderbilt, *Reviews of Modern Physics* **84**, 1419 (2012).
- [3] W. H. Press, S. A. Teukolsky, W. T. Vetterling, and B. P. Flannery, *Numerical Recipes 3rd Edition: The Art of Scientific Computing* (Cambridge University Press, 2007).
- [4] V. I. Anisimov, F. Aryasetiawan, and A. I. Lichtenstein, *Journal of Physics: Condensed Matter* **9**, 767 (1997).
- [5] H. Jiang, R. I. Gomez-Abal, P. Rinke, and M. Scheffler, *Physical Review B* **82**, 045108 (2010).
- [6] R. M. Martin, L. Reining, and D. M. Ceperley, *Interacting Electrons: Theory and Computational Approaches* (2016).
- [7] P. Giannozzi, S. Baroni, N. Bonini, M. Calandra, R. Car, C. Cavazzoni, D. Ceresoli, G. L. Chiarotti, M. Cococcioni, I. Dabo, A. D. Corso, S. d. Gironcoli, S. Fabris, G. Fratesi, R. Gebauer, U. Gerstmann, C. Gougoussis, A. Kokalj, M. Lazzeri, L. Martin-Samos, N. Marzari, F. Mauri, R. Mazzarello, S. Paolini, A. Pasquarello, L. Paulatto, C. Sbraccia, S. Scandolo, G. Sclauzero, A. P. Seitsonen, A. Smogunov, P. Umari, and R. M. Wentzcovitch, *Journal of Physics: Condensed Matter* **21**, 395502 (2009).
- [8] K. Nakamura, Y. Yoshimoto, Y. Nomura, T. Tadano, M. Kawamura, T. Kosugi, K. Yoshimi, T. Misawa, and Y. Motoyama, *Computer Physics Communications* **261**, 107781 (2021).
- [9] D. R. Hamann, *Physical Review B* **88**, 085117 (2013).
- [10] M. J. van Setten, M. Giantomassi, E. Bousquet, M. J. Verstraete, D. R. Hamann, X. Gonze, and G. M. Rignanese, *Computer Physics Communications* **226**, 39 (2018).
- [11] A. Togo and I. Tanaka, *Scripta Materialia* **108**, 1 (2015).
- [12] A. Togo, *Journal of the Physical Society of Japan* **92**, 012001 (2023).
- [13] T. Maekawa, K. Kurosaki, and S. Yamanaka, *Journal of Alloys and Compounds* **426**, 46 (2006).
- [14] Y. C. Lan, X. L. Chen, and M. He, *Journal of Alloys and Compounds* **354**, 95 (2003).
- [15] N. Marzari, D. Vanderbilt, A. De Vita, and M. C. Payne, *Physical Review Letters* **82**, 3296 (1999).
- [16] T. Chiarotti, N. Marzari, and A. Ferretti, *Physical Review Research* **4**, 013242 (2022).